

Towards Learning to Imitate from a Single Video Demonstration

Glen Berseth
Florian Golemo
Christopher Pal

GBERSETH@IRO.UMONTREAL.CA
GOLEMOFL@MILA.QUEBEC
CHRISTOPHER.PAL@SERVICENOW.COM

Abstract

Agents that can learn to imitate given video observation – *without direct access to state or action information* are more applicable to learning in the natural world. However, formulating a reinforcement learning (RL) agent that facilitates this goal remains a significant challenge. We approach this challenge using contrastive training to learn a reward function comparing an agent’s behaviour with a single demonstration. We use a Siamese recurrent neural network architecture to learn rewards in space and time between motion clips while training an RL policy to minimize this distance. Through experimentation, we also find that the inclusion of multi-task data and additional image encoding losses improve the temporal consistency of the learned rewards and, as a result, significantly improves policy learning. We demonstrate our approach on simulated humanoid, dog, and raptor agents in 2D and a quadruped and a humanoid in 3D. We show that our method outperforms current state-of-the-art techniques in these environments and can learn to imitate from a single video demonstration.

Keywords: Reinforcement Learning, Deep Learning, Imitation Learning

1. Introduction

Imitation learning gives agents the ability to reproduce other agents’ behaviours and skills through demonstrations (Blakemore and Decety, 2001). These demonstrations act as a type of explicit communication, informing the agent of the desired behaviour. However, real-world agents such as robots do not generally have access to the type of information needed by many imitation learning methods, such as internal state information or the executed actions of a demonstration. We also want a solution that can learn to imitate even if an observed agent has a different appearance or dynamics in the demonstration compared to the agent that is tasked with learning from the demonstration. In the same way that human children can learn to imitate adults by observing them, we want more versatile agents who can learn to imitate desired behaviours, given only

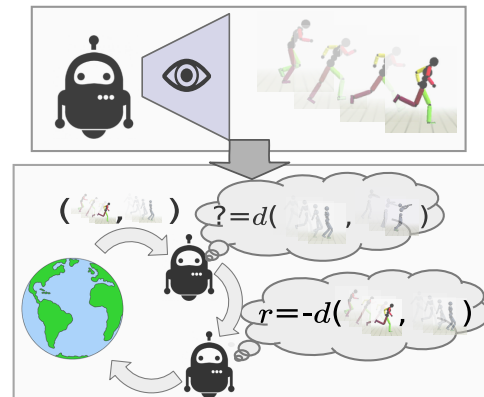


Figure 1: The agent visually observes a behaviour then collects experience to train a distance function $d()$, used to learn how to reproduce that behaviour with RL.

a few examples. This type of visual imitation is depicted in [Figure 1](#) with an agent that learns and minimizes the distance between visual demonstration. If we can construct agents that can learn to imitate from such easy to obtain but noisy data, these agents will have access to a large amounts of demonstrations in order to learn a wide variety of skills and be more flexible for learning via imitation in the real world.

While imitating a behaviour from observation is natural to many agents in the real world, it poses many learning challenges. Behaviour cloning (BC) methods often require expert action data making them impossible to use in more natural problem settings where only image observations are available. Also, in the real world, the demonstration agent often has different dynamics, meaning that an exact copy of the demonstration is impossible, and the learning agent must do its best to replicate the observed behaviour under *its own* dynamics. How can we train an agent to reliably imitate another agent with potentially different dynamics given only image data from the demonstration agent? If we can learn a well-formed and smooth distance between observed behaviours, it can be used as the reward for a reinforcement learning agent. However, given the partially observed nature of the demonstration data, learning a reasonable distance function can be challenging. To compensate for limited and noisy data, a method that allows us to incorporate additional offline data, potentially from other behaviours/tasks, will increase data efficiency while training a model that understands the comparative landscape of a larger behaviour space.

To realize the data-efficient and task-independent method described above, we train a recurrent Siamese comparator to capture the partial information from each image and use this comparator to compute distances used for rewards for an RL agent. We train this comparator model with off policy data to learn distances between sequences of images. This offline training makes it possible to pretrain and include data from additional behaviours/tasks to increase model robustness. Auto-encoding losses are added, shown in [Fig. 2a](#), at different levels of granularity to increase the smoothness of the learned distance landscape. As we show in our results, this robustness and smoothness improves both training efficiency and final policy quality. Our model learns two latent distance predictors in parallel. These two latent distance predictors are shown in [Fig. 2b](#) and allow us to compute distances between individual images and between sequences. The *image-to-image* latent distance rewards the agent for precisely matching the example behaviour. In contrast, the learned *sequence-to-sequence* latent representation provides additional reward when the agent is not just matching the desired behaviour exactly, but also when the agent is replicating portions portions of the observed demonstration, for example, if the agent currently has different timing than the demonstration.

Our contribution consists of proposing an approach to visual imitation learning for RL based on visual comparisons and the specific architectures and training procedures discussed in more detail throughout the paper. We showcase that our approach enables agents to learn a large variety of challenging behaviours that include walking, running and jumping. We perform experiments for multiple simulated robots in both 2D and 3D, including recent sim2real quadruped robots and a humanoid with 38 degrees of freedom (DoF). For many of these imitation tasks VIRL is able to imitate the given skill using only a single observed demonstration.

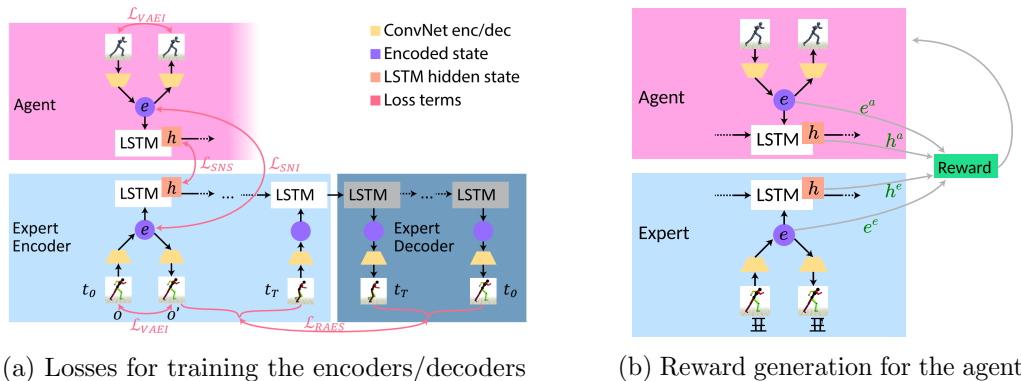


Figure 2: VIRL learns a distance function (2a) and then uses that distance function as a reward function for RL (2b). At the current timestep, observations (\mathbf{o}) of the reference motion and the agent are encoded (\mathbf{e}) and fed into Long Short-Term Memory (LSTM)s (leading to hidden states \mathbf{h}). Fig. 2a shows how the reward model is trained using both Siamese and Autoencoder (AE) losses. There are: Variational Autoencoder (VAE) reconstruction losses on static images (\mathcal{L}_{VAEI}), sequence-to-sequence AE losses (\mathcal{L}_{RAES}), one for the reference and one for the agent (which we do not show in pink to simplify the figure). There is a Siamese loss between encoded images (\mathcal{L}_{SNI}) and a Siamese loss that is computed between encoded states over time (\mathcal{L}_{SNS}). Fig. 2b shows how the reward is calculated **at every timestep** using the combination of the learned encodings.

2. Related Work

We group the most relevant prior work based on the type and quantity of data needed to perform imitation learning. The first group consists of GAIL (Ho and Ermon, 2016) and related methods, which require access to expert policies, states, actions, and require large quantities of expert data. In the second group, the need for expert action data is relaxed in methods like Generative Adversarial Imitation Learning from Observation (GAILfO) (Torabi et al., 2018b), but still, require an expert policy to generate data from repeatedly. The third group avoids the need for ground truth states favouring images that are easier to obtain (Brown et al., 2019, 2020). These methods still require many examples of data from a policy trained on the agent in the same simulation with the same dynamics. Lastly, in a fourth group, the need for multiple demonstrations and matching dynamics is relaxed as in methods such as Time-Contrastive Network (TCN) (Sermanet et al., 2018) and ours.

Imitation learning. Generative Adversarial Imitation Learning or Generative Adversarial Imitation Learning (GAIL) (Ho and Ermon, 2016), uses the well-known Generative Adversarial Network (GAN) (Goodfellow et al., 2014) framework and applies it in the context of learning an RL policy. In GAIL, the GAN’s discriminator is trained with positive examples from expert trajectories and negative examples from the current policy. However, using a discriminator is only one possible way of measuring the probability of that agent’s behaviour matching the expert (Abbeel and Ng, 2004; Argall et al., 2009; Finn et al., 2016; Brown et al., 2019). Given a vector of features distance-based imitation learning aims to find an optimal transformation that computes a more meaningful distance between expert demonstrations and agent trajectories. Previous work has explored the area of state-based distance functions,

but most rely on the availability of an expert policy to continuously sample data (Ho and Ermon, 2016; Merel et al., 2017). In the section hereafter, we demonstrate how VIRL learns a more stable distance-based reward over sequences of images (as opposed to states) and without access to actions or expert policies.

Imitation without action data. For learning from demonstrations (LfD) problems, the goal is to replicate the behaviour of an expert π_E . GAILfO (Torabi et al., 2018b) has been proposed as an extension of GAIL that does not require data on the expert actions. However, GAILfO and other recent works in this area require access to an expert policy for sampling additional states for training (Sun et al., 2019; Yang et al., 2019). By comparison, our method can work with a single fixed demonstration example with different dynamics. Other recent work uses behavioural cloning (BC) to learn an inverse dynamics model to estimate the actions used via maximum-likelihood estimation (Torabi et al., 2018a). Still, BC often needs many expert examples and tends to suffer from state distribution mismatch issues between the *expert* policy and *student* (Ross et al., 2011a).

Additional works learn implicit models of distance (Yu et al., 2018; Finn et al., 2017; Sermanet et al., 2017; Merel et al., 2017; Edwards et al., 2019; Sharma et al., 2019) they require large amounts of demonstration data and none of these explicitly learn a sequential model considering the demonstration timing. The work in (Wang et al., 2017; Li et al., 2017; Peng et al., 2018b, 2021) includes a more robust GAIL framework with a new model to encode motions for few-shot imitation. However, they need access to an expert policy to sample additional data. In this work, we train recurrent Siamese networks (Chopra et al., 2005) to learn more meaningful distances between videos. Other work uses state-only demonstration to out-perform the demonstration data but requires many demonstrations and ranking information to be successful (Brown et al., 2019, 2020). We show results on more complex 3D tasks and additionally model distance in time, i.e. due to the embedding of the entire sequence, our model can compute meaningful distances between agent and demonstration even if they deviate in time.

Imitation from images. Some works like Sermanet et al. (2017); Finn et al. (2017); Liu et al. (2017); Dwibedi et al. (2018), use image-based inputs instead of states but require on the order of hundreds of demonstrations. Further, these models only address spatial alignment, matching joint positions/orientations to a single state, and can not implicitly provide an additional signal related to temporal ordering between expert demonstration and agent motion like our recurrent sequence model does. Other works that imitate only image-based information like (Pathak et al., 2018) do so between goal states.

Imitation from few images with different dynamics. Time-Contrastive Networks (TCNs) (Sermanet et al., 2018) proposes a method to use metric learning to embed *simultaneous viewpoints* of the same object. They use TCN embeddings as *features in the system state* which are provided to the PILQR (Chebotar et al., 2017) reinforcement learning algorithm, which combines model-based learning, linear time-varying dynamics and model-free corrections. In contrast, our Siamese network-based approach *learns the reward* for an arbitrary subsequent RL algorithm. Our method does not rely on multiple views, and we use an recurrent neural network (RNN)-based autoencoding approach to regularize the distance computations used for generated rewards. These choices allow VIRL to achieve performance gains over TCN, as shown in Section 5.

3. Preliminaries

In this section we provide a very brief review of the fundamental methods that the method in the paper is based on. reinforcement learning (RL) is formulated within the framework of an Markov decision process (MDP) where at every time step t , the world (including the agent) exists in a state $s_t \in S$, where the agent is able to perform actions $a_t \in A$ and where states and actions are discrete. The action to take is determined according to a policy $\pi(a_t|s_t)$ which results in a new state $s_{t+1} \in S$ and reward $r_t = R(s_t, a_t, s_{t+1})$ according to the transition probability function $P(s_{t+1}|s_t, a_t)$. The policy is optimized to maximize the future discounted reward $\mathbb{E}_{r_0, \dots, r_T} \left[\sum_{t=0}^T \gamma^t r_t \right]$, where T is the max time horizon, and γ is the discount factor. The formulation above generalizes to continuous states and actions, which is the situation for the agents we consider in our work.

Imitation Learning. Imitation learning is typically cast as the process of training a new policy to reproduce expert policy behaviour. Behaviour cloning is a fundamental method for imitation learning. Given an expert policy π_E possibly represented as a collection of trajectories $\tau = \langle (s_0, a_0), \dots, (s_T, a_T) \rangle$ a new policy π can be learned to match this trajectory using supervised learning and maximizing the expectation $\mathbb{E}_{\pi_E} \left[\sum_{t=0}^T \log \pi(a_t|s_t, \theta_\pi) \right]$. While this simple method can work well, it often suffers from distribution mismatch issues leading to compounding errors as the learned policy deviates from the expert’s behaviour (Ross et al., 2011b). Inverse reinforcement learning avoids this issue by extracting a reward function from observed optimal behaviour (Ng et al., 2000). In our approach, we learn a distance function that allows an agent to compare an observed behaviour to its current behaviour to define its reward r_t at a given time step. Our comparison is concerning a reference activity, but the comparison network can train across a collection of different behaviours. Further, we do not assume the example data to be optimal. See Appendix 7.2 for further details of the connections of our work to inverse reinforcement learning.

Variational Auto-encoders VAEs are a popular approach for learning lower-dimensional representations of a distribution (Kingma and Welling, 2014). A VAE consists of two parts, an encoder q_ϕ , with parameters ϕ and a decoder p_ψ with parameters ψ . The encoder maps inputs \mathbf{x} , to a latent encoding \mathbf{z} and in turn the decoder transforms \mathbf{z} back to the input space $p_\psi(\mathbf{x}|\mathbf{z})$. The model parameters for both ϕ and ψ are trained jointly to maximize

$$\mathcal{L}_{VAE}(s, \phi, \psi) = -D_{KL}(q_\phi(\mathbf{z}|\mathbf{x})||p(\mathbf{z})) + \mathbb{E}_{q_\phi(\mathbf{z}|\mathbf{x})}[\log p_\psi(\mathbf{x}|\mathbf{z})], \quad (1)$$

where D_{KL} is the Kullback-Leibler divergence, $p(\mathbf{z})$ is a prior distribution over the latent space. The encoder q_ϕ , or inference model takes the form of a diagonal covariance multivariate Gaussian distribution $q_\phi = \mathcal{N}(\mu_\phi(\mathbf{x}), \sigma^2(\mathbf{x}))$, where the mean, $\mu_\phi(\mathbf{x})$ is typically given by a deep neural network.

Sequence to sequence models can be used to learn the conditional probability of one sequence given another $p(y_0, \dots, y_{T'}|x_0, \dots, x_T)$, where $\mathbf{x} = x_0, \dots, x_T$ and $\mathbf{y} = y_0, \dots, y_{T'}$ are sequences. Here we will use extensions of encoder-decoder structured, autoencoding recurrent neural networks which learn a latent representation \mathbf{h} that compresses the information in x_0, \dots, x_T . Our model for decoding the sequence \mathbf{y} can then be written as

$$p(\mathbf{y}) = p(y_0|\mathbf{h}) \prod_{t=1}^T p(y_t|\{y_0, \dots, y_{t-1}\}, \mathbf{h}). \quad (2)$$

This method works for learning compressed representations for transfer learning (Zhu et al., 2016) and 3D shape retrieval (Zhuang et al., 2015). In our case, this type of autoencoding can help regularize our model by forcing the encoding to contain all the information needed to reconstruct the trajectory.

4. Visual Imitation with Reinforcement Learning

High-level Overview We train a system to give an RL agent a reward depending on how closely it imitates the demonstration. We interleave training a learned distance function with having the agent collect additional experience while using the learned distance function to provide rewards for the RL agent. The learned distance consists of several components and losses that we describe in this section. Coarsely, we encode the observations of both the agent and the demonstration with VAEs and LSTMs, which we decode in inverse order. A Contrastive loss (“Siamese Network triplet loss”) is used to train the distance model to predict low distances for similar frames/sequences and larger distances between incorrect frames and shuffled/perturbed sequences¹ (Hadsell et al., 2006). At every timestep, the reward for the agent’s policy is a function of the LSTM’s hidden state for the agent and the demonstration. In what follows, we first detail how we construct and train the Siamese encoder/decoder networks, then how the encodings from the learned networks can be combined to provide rewards for the agent, and finally, we introduce a set of data augmentation techniques that improve model and policy training resulting in a more robust learned reward function and final policy.

The Sequence Encoder/Decoder Networks Figure 2a shows an outline of the network design. A single convolutional network Conv^e is used to transform observations (images) at every time t of the demonstration \mathbf{o}_t^e to an encoding vector e_t^e . After the sequence of observations is passed through Conv^e it is now an encoded sequence $\langle e_0^e, \dots, e_t^e \rangle$, this sequence is fed into the LSTM^e until a final encoding is produced h_t^e . This same process is performed for a copy of the LSTM^a producing h_t^a for the agent’s observations \mathbf{o}^a . The final encoding of the demonstration is fed into a separate $\text{LSTM}^{\hat{e}}$ which generates a series of decoded latent representations $\langle e_0^{\hat{e}}, \dots, e_t^{\hat{e}} \rangle$ which are then decoded back to images with a deconvolutional network $\text{Deconv}^{\hat{e}}$. The same process is applied to the agent with $\text{LSTM}^{\hat{a}}$, latent representations $\langle e_0^{\hat{a}}, \dots, e_t^{\hat{a}} \rangle$, and deconvolutional network $\text{Deconv}^{\hat{a}}$, respectively.

Loss Terms A siamese loss between a full encoded sequence of the demonstration h_t^e and a sequence of the agent h_t^a forces not just individual frames but the representation of entire sequences to match if they are from the same policy. This siamese network sequence loss \mathcal{L}_{SNS} is defined in Eq.3. A frame-by-frame siamese loss between e_t^e of the demonstration and e_t^a of the agent encourages individual frames to have similar encodings as well. This

1. Which is different from existing methods such as GAILfO in that we enforce similarity over sequences, not just individual state transitions. This training allows us to align the demonstration with the agent temporally.

siamese network image loss \mathcal{L}_{SNI} uses Eq.3 as well, but is trained over pairs of images. We define The Siamese Network loss (both for images and sequences) as:

$$\mathcal{L}_{SNX}(\mathbf{o}_i, \mathbf{o}_p, y; \phi) = y * \|f(\mathbf{o}_i; \phi) - f(\mathbf{o}_p; \phi)\| + ((1-y) * (\max(\rho - (\|f(\mathbf{o}_i; \phi) - f(\mathbf{o}_n; \phi)\|), 0))), \quad (3)$$

where $y \in [0, 1]$ is the indicator for positive/negative samples. When $y = 1$, the pair is positive, and the distance between current observation \mathbf{o}_i to positive sample \mathbf{o}_p should be minimal. When $y = 0$, the pair is negative, and the distance between \mathbf{o}_i and negative example \mathbf{o}_n should be increased. We compute this loss over batches of data that are half positive and half negative pairs. The margin ρ is used as an attractor or anchor to pull the negative example output away from \mathbf{o}_i and push values towards a $[0, 1]$ range. $f(\cdot)$ computes the output from the underlying network (i.e. Conv or LSTM). The data used to train the Siamese network is a combination of observation trajectories $\mathbf{O} = \langle \mathbf{o}_0, \dots, \mathbf{o}_T \rangle$ generated from simulating the agent in the environment and the demonstration. For our recurrent model the observations $\mathbf{O}_p, \mathbf{O}_n, \mathbf{O}_i$ are sequences. We additionally train the encoding of a single observation of either agent or expert at a given timestep using the VAE loss \mathcal{L}_{VAE} from Eq.1. Lastly, the entire sequence of observations of both the agent and expert is encoded and then decoded back separately, as shown in Fig. 13, and the LSTMs are trained with the loss \mathcal{L}_{RAES} from Eq.2. We found using these image- and sequence-autoencoders important to improve latent space conditioning. This combination of image-based and sequence-based losses assists in compressing the representation while ensuring intermediate representations remain informative. The combined loss to train the model on a *positive* pair of sequences ($y = 1$) is:

$$\begin{aligned} \mathcal{L}_{VIRL}(\mathbf{O}_i, \mathbf{O}_p, y; \phi, \psi, \omega, \rho) = & \underbrace{\lambda_1 \mathcal{L}_{SNS}(\mathbf{O}_i, \mathbf{O}_p, y; \phi, \omega)}_{\text{Contrastive sequence loss}} + \underbrace{\lambda_2 \left[\frac{1}{T} \sum_{t=0}^T \mathcal{L}_{SNI}(\mathbf{O}_{i,t}, \mathbf{O}_{p,t}, y; \phi) \right]}_{\text{Contrastive frame loss}} + \\ & \underbrace{\lambda_3 [\mathcal{L}_{RAES}(\mathbf{O}_i; \phi, \psi, \omega, \rho) + \mathcal{L}_{RAES}(\mathbf{O}_p; \phi, \psi, \omega, \rho)]}_{\text{Recurrent autoencoder loss (full sequence)}} + \\ & \underbrace{\lambda_4 \left[\frac{1}{T} \sum_{t=0}^T [\mathcal{L}_{VAEI}(\mathbf{O}_{i,t}; \phi, \psi) + \mathcal{L}_{VAEI}(\mathbf{O}_{p,t}; \phi, \psi)] \right]}_{\text{Variational autoencoder loss (individual frames)}}. \end{aligned} \quad (4)$$

Where the relative weights of the different terms are $\lambda_{1:4} = \{0.7, 0.1, 0.1, 0.1\}$, the image encoder convnet is ϕ , the image decoder ψ , the recurrent encoder ω , and the recurrent decoder ρ .

Reward Calculation The model trained using the loss function described above is used to calculate the distance between two sequences of observations seen up to time t as $d(\mathbf{O}^e, \mathbf{O}^a; \phi, \omega) = \|f(\mathbf{o}_{0:t}^e; \omega) - f(\mathbf{o}_{0:t}^a; \omega)\| + \|f(\mathbf{o}_t^e; \phi) - f(\mathbf{o}_t^a; \phi)\|$ and the reward as $r(\mathbf{o}_{0:t}^e, \mathbf{o}_{0:t}^a) = -d(\mathbf{O}^e, \mathbf{O}^a; \phi, \omega)$. During RL training, we compute a distance given the sequence observed so far in the episode. In Sec. 5.2 we experimentally show the importance of each distance for imitation learning.

Training the Model Details of the algorithm used to train the distance metric and policy are in Alg. 1. We consider a variation on the typical RL environment that produces three different outputs, two for the agent and 1 for the demonstration and no reward. The first is the internal robot pose, which we shall refer to as the state s_t . The second and third are images of the agent, or observation \mathbf{o}_t^e and the demonstration \mathbf{o}_t^a , shown in Fig. 2b. The images are used with the distance metric to compute the similarity between the agent and the demonstration. We train the agent’s policy using the Trust-Region Policy Optimization (TRPO) algorithm (Schulman et al., 2015) using the reward signal described above. While the policy is trained online (line 13) the learned distance function is trained over a large collection of off-policy data (line 13). The use of off-policy training increases the LSTM-based distance function’s training efficiency. The off-policy training also allows us to train the distance function using data from other tasks to increase the robustness of the model while fine-tuning on the current task, as we will describe in Section 5.2.

Algorithm 1 Learning Algorithm

```

1: Initialize parameters  $\theta_\pi, \theta_d, D \leftarrow \{\}$ 
2: while not done do
3:   for  $i \in \{0, \dots, N\}$  do
4:      $\{s_t, \mathbf{o}_t^e, \mathbf{o}_t^a\} \leftarrow \text{env.reset}(), \tau^i \leftarrow \{\}$ 
5:     for  $t \in \{0, \dots, T\}$  do
6:        $a_t \leftarrow \pi(\cdot | s_t, \theta_\pi)$ 
7:        $\{s_{t+1}, \mathbf{o}_{t+1}^e, \mathbf{o}_{t+1}^a\} \leftarrow \text{env.step}(a_t)$ 
8:        $\tau_t^i \leftarrow \{s_t, \mathbf{o}_t^e, \mathbf{o}_t^a, a_t\}$ 
9:        $\{s_t, \mathbf{o}_t^e, \mathbf{o}_t^a\} \leftarrow \{s_{t+1}, \mathbf{o}_{t+1}^e, \mathbf{o}_{t+1}^a\}$ 
10:    end for
11:     $\mathbf{r}_{0:t}^i \leftarrow -d(\mathbf{o}_{0:t+1}^e, \mathbf{o}_{0:t+1}^a | \theta_d)$ 
12:  end for
13:   $D \leftarrow D \cup \{\tau^0, \dots, \tau^N, \}$ 
14:  Update  $d(\cdot)$  parameters  $\theta_d$  using  $D$ 
15:  Update  $\theta_\pi$  with  $\{\{\tau^0, \mathbf{r}^0\}, \dots, \{\tau^N, \mathbf{r}^N\}\}$ 
16: end while

```

4.1 Unsupervised Data Labelling and Generation

To construct *positive* and *negative* pairs for training, we make use of time information and adversarial information. We use timing information where observations at similar times in the same sequence are often correlated, and observations at different times are less likely to be similar. We use these ideas to provide labels for the positive and negative pairs to train the Siamese network. Positive pairs are created by adding Gaussian noise with $\sigma = 0.05$ to the images in the sequence, duplicating, or shifting random frames of the sequences. Negative pairs are created by shuffling, cropping or reversing one sequence. Additionally, we include *adversarial* pairs where positive pairs come from the same distribution, for example, two motions for the agent or two from the demonstration at different times. Negative pairs then include one from the expert and one from the agent. Additional details on how the shuffling, swapping, and the use of adversarial pairs are available in the Appendix 7.7.

Data Augmentation We apply several data augmentation methods to produce additional data variation for training the distance metric. Using methods analogous to the cropping and warping methods popular in computer vision (He et al., 2015) we randomly *crop* sequences and randomly *warp* the demonstration timing. The *cropping* is performed by removing later portions of the training sequences during batch updates. This allows the distance function to quickly learn good distances between observations early in the episode. This cropping is denoted as Early Episode Sequence Priority (EESP) where the probability of cropping out a window in the sequence \mathbf{x} at i is $p(i) = \frac{\text{len}(\mathbf{x})-i}{\sum_i}$, increases the likelihood of

cropping earlier in the sequence. As the agent improves, the average length of each episode increases, and so will the average length of the cropped window. The motion *warping* is done by replaying the demonstration motion at different speeds. This allows for training the distance function to recognize that, for example, a walking motion with one step in it and another with two steps are still examples of a walk. Last, we use Reference State Initialization (RSI) (Peng et al., 2018a), where we generate the initial state of the agent and expert randomly from the demonstration. With this property, the environment functions as a form of memory replay. The environment allows the agent to go back to random points in the demonstration as if replaying a remembered demonstration and collect new data from that point in the demonstration. The experiments in Sec. 5.2 show the importance of these augmentation methods in terms of improving the robustness of the learned comparator and resulting policy.

5. Experiments, Results and Analysis

We evaluate VIRL compared to previous methods in terms of sample efficiency and task solving capability. The comparison is over a collection of different simulation environments. In these simulated robotics environments, we task the agent with imitating a given reference video demonstration. Each simulation environment provides a hard-coded reward function based on the agent’s pose to evaluate the policy quality independently. The imitation environments include challenging and dynamic tasks for humanoid, dog and raptor robots. Some example tasks are running, jumping, trotting, and walking, shown in Fig. 3 and Fig. 4. The demonstration \mathbf{o}_t^e the agent uses for visual imitation learning is produced from a clip of motion capture data for each task. The motion capture data animates a kinematically controlled robot in the simulation for capturing video. Because the demonstration is kinematically generated the agent also needs to learn how to bridge the gap between the different dynamics in the demonstration that may be impossible to exactly reproduce. We convert the images captured from the simulation to 48×48 grey-scale images. Third-person image data is often not available during test time; therefore, the agent’s policy instead receives the environment state, as the link distances and velocities relative to the robot’s centre of mass (COM).

2D Imitation Tasks The first group of evaluation environments contain a set of agents with difference morphologies. In Figure 3 we show images from the 2D humanoid, dog and raptor environment. In these environments the rendering and simulation is in 2D, reducing the complexity of the control system and dynamics, allowing for faster training times.

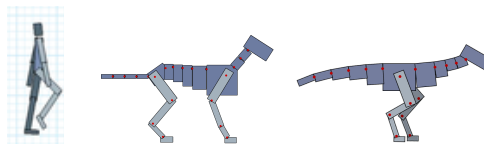


Figure 3: Frames from the humanoid2d, dog2d, and raptor2d environments used in the experiments.

3D Imitation Tasks For further evaluation, we compare performance on 3D humanoid and two quadrupedal robot simulators used for Sim2Real research, the Laikago (Peng et al., 2020) and Pupper (Kau et al., 2020). The humanoid3d environment has multiple tasks that can be solved and used to generate data from other tasks for training the distance metric. These tasks include: walking, running, jogging, front-flips, back-flips, dancing,

jumping, punching and kicking). To perform the data augmentation described in Section 4.1 we also construct data from a modified version of each task with a randomly generated speed modifier $\omega \in [0.5, 2.0]$ e.g. walking-dynamic-speed, which warps the demonstration timing. This additional data provides a richer understanding of distances in space and time with the distance metric. As we will show later in this section, VIRL learns policies that produce similar behaviour to the demonstration across these diverse tasks. We show example trajectories from the learned policies in Fig. 4 and in the supplemental Video. It takes 5 – 7 days to train each policy in these results on a 16 core machine with an Nvidia GTX1080 GPU.

Baselines We compare VIRL to two baselines that learn distances in observation space. The first is GAILfO (Torabi et al., 2018b) that trains a GAN to differentiate between images from the demonstration and images from the agent. The other is TCN, an image-to-image only Siamese model (Nair et al., 2018). These methods have been used to perform types of imitation from observation before. However, as we will see, they either require a significant amount of data to train or result in lower quality reward functions and, as a result, lower quality policies.

5.1 Learning Performance

In Figure 5 we present results across different agent types including the 2D walking humanoid in Section 5a, a 2D trotting dog in Fig. 5b, and a 2D Raptor in Fig. 5c. We compare VIRL directly with both GAILfO and TCNs – the strongest comparable prior method. These results shows that VIRL performs better than both GAILfO and TCN. VIRL is able to provide a denser reward signal due to the LSTM based distance that can express similarity between motion styles. While TCN is simpler, not using an LSTM model, it does not provide as rich of a reward signal for the agent to learn from. As a result the learned reward can often be more sparse, slowing down learning. Similarly, GAILfO has difficulty learning a robust and smooth distance function with the little demonstration data available. This leads to very jerky motion or agent’s that stand still, matching the average pose of the demonstration, both of which are contained in the demonstration distribution but do not capture sequential temporal behaviour well.

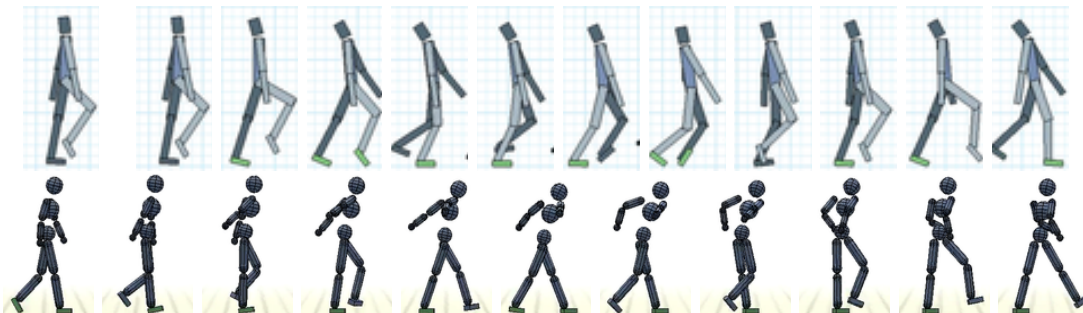


Figure 4: Frames of the agent’s motion after training on humanoid2d and humanoid3d walking. Additionally, the dog, raptor, zombie walk, run and jumping policy can be found on the project website: <https://sites.google.com/view/virl1>.

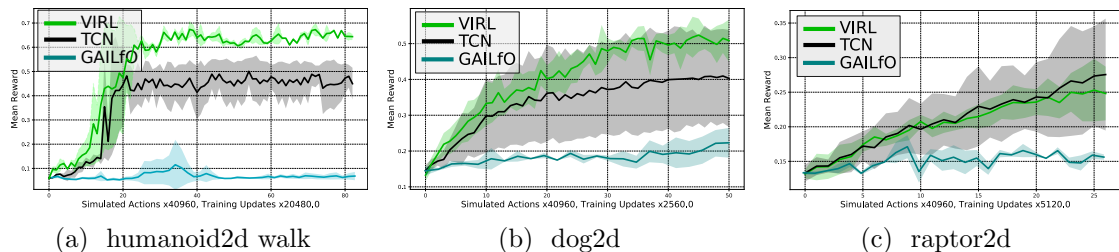


Figure 5: Comparisons of VIRL, TCN and GAILfO with (a) the humanoid2d, (b) the 2D dog agent, and (c) the 2D raptor agent. GAILfO struggles to show improvement on these tasks. TCN does make progress on these imitation tasks but the performance is not as good as VIRL. The results show average performance over 4 randomly seeded policy training simulations.

In Figure 6 we compare VIRL with TCNs, across many different and more challenging humanoid3d tasks in Fig. 6(a-d). Across these experiments, we observe that our method learns faster and produces higher value policies. In particular, we find that VIRL does very well compared to TCNs, which represents the strongest prior approach capable of performing this task of which we are aware. The humanoid3d tasks are particularly challenging as they have high control dimensionality causing the agent to deviate from the desired imitation behaviour easily. These tasks also contain higher levels of partial observability compared to the 2D experiments. In these environments the temporal distance in VIRL provides a

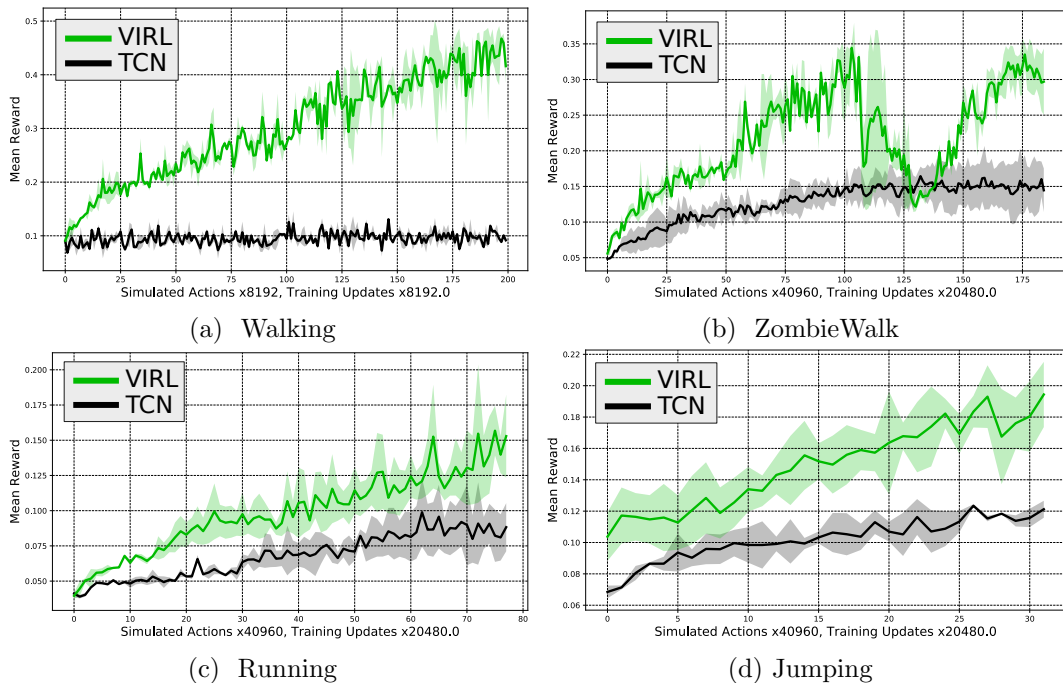


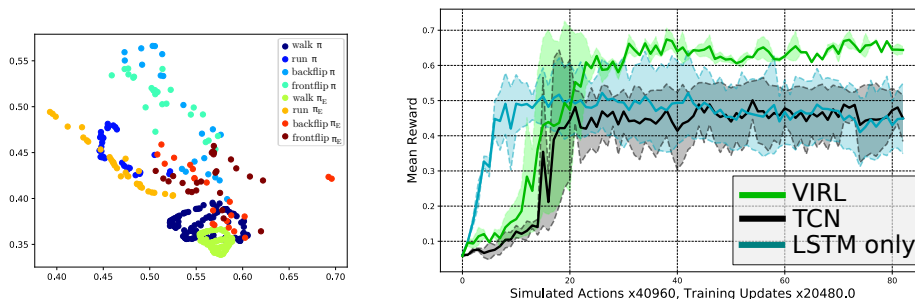
Figure 6: 3D Humanoid motion imitation experiments: Comparisons of VIRL with TCNs. These results show the average performance over 4 randomly seeded policy training simulations.

crucial additional reward signal that helps the agent match the style of the motion early on in training despite the observations that only contain partial information.

5.2 Analysis and Ablation

Sequence Encoding Using the learned sequence encoder, we compute the encodings across a collection of different motions and create a t-distributed Stochastic Neighbor Embedding (t-SNE) embedding of the encodings (Maaten and Hinton, 2008). In Fig. 7a we plot motions both generated from the learned policy π and the expert trajectories π_E . Overlaps in specific areas of the space for similar classes across learned π and expert π_E data indicate a well-formed distance metric that does not separate expert and agent examples. There is also a separation between motion classes in the data, and the cyclic nature of the walking cycle is visible.

Ablation In Fig. 7b we compare the importance of the spatial distance $\|f(\mathbf{o}_t^e; \phi) - f(\mathbf{o}_t^a; \phi)\|^2$ and temporal LSTM distance $\|f(\mathbf{o}_{0:t}^e; \omega) - f(\mathbf{o}_{0:t}^a; \omega)\|^2$ components of VIRL. Using the recurrent representation alone (LSTM only) allows learning to progress quickly but can lead to difficulties informing the policy of how to match the desired demonstration more precisely. On the other hand, using only the encoding between single frames as is done with TCN, slows learning due to little reward when the agent quickly becomes out-of-sync with the demonstration behaviour. The best result is achieved by combining the representations from these two models (VIRL).



(a) t-SNE embedding (humanoid3d)

(b) Distance function ablation

Figure 7: (a) t-SNE embedding that shows VIRL’s learned distance landscape. (b) Comparison between combining different learned distance models. The combination of spatial and temporal distances leads to the best result (VIRL).

Data augmentation comparisons. We conduct ablation studies for learning policies for 3D humanoid control in Fig. 8a and 8b. We compare the effects of data augmentation methods, network models and the use of additional data from other tasks to train the Siamese network (24 additional tasks such as back-flips, see appendix 7.3 for more details on these tasks). We also compared using different length sequences for training, shorter (where the probability of the length decays linearly), uniform random and max length available. For these more complex and challenging three-dimensional humanoid (humanoid3d) control problems, the data augmentation methods, including EESP, increase average policy quality marginally compared to the importance of using multi-task data, this is likely related to

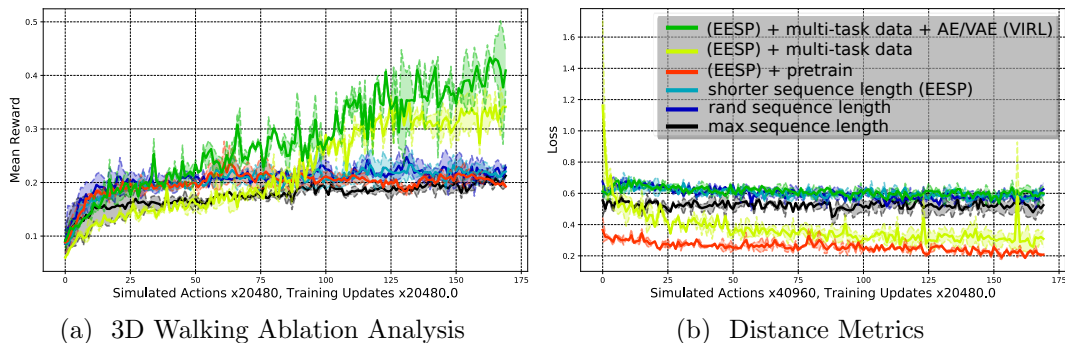


Figure 8: (a) Ablation analysis of VIRL on the humanoid3D environment showing the mean reward over 5 random seeds. The legend is the same as (b), where we examine the impact on our loss under the different distance metrics resulting from the ablation analysis. We find that including multi-task data (only available for the humanoid3D) and both the VAE and recurrent AE losses provide the most high-performing models.

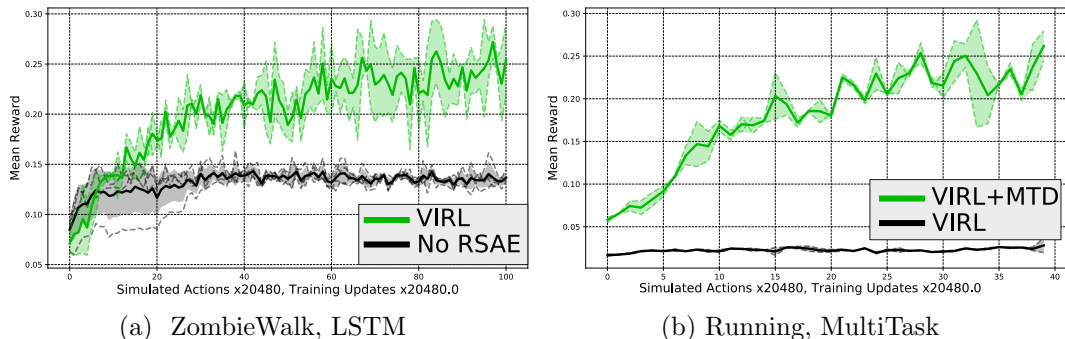


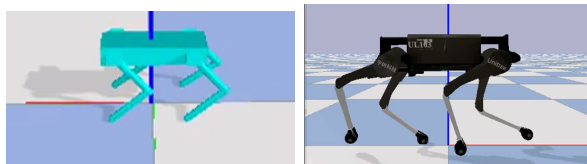
Figure 9: (a) Ablating the recurrent autoencoder from VIRL (i.e. No RSAE in the figure) impairs the ability to learn how to walk like a Zombie. (b) Here, further we see how multi-task training data helps learn better policies for running (away from Zombies if desired).

the increased partial observability of these tasks. However, the addition of the auto-encoding losses to VIRL results in the quickest learning and highest value policies.

The experiment in Fig. 9a highlights the improvement to our method afforded by the recurrent sequence autoencoder (RSAE) model component from Eq. 4 that forces the encoding to contain enough information to decode the video sequence. While the experiment in Fig. 9b shows the dramatic improvement achieved when we include offline multi-task data for training the distance function. These methods are combined together to provide the substantial learning performance increases across environments for VIRL. Further analysis is available in the Appendix, including additional comparison with TCN in Fig. 15(a-b) and details on training the distance model.

Sim2Real for Quadruped Robots We use VIRL to train policies for two simulated quadrupeds shown in Fig. 10. These environments are used for Sim2Real transfer. With these trained policies, it is possible to transfer the VIRL policies trained from a single demonstration, to a real robot. The resulting behaviours are available at: <https://sites.google.com/view/virl1>.

Figure 10: Pupper and Laikago agents, both of which are difficult platforms to learn policies on since they tumble easily and expert demonstrations are hard to obtain.



We find that the Laikago environment is particularly challenging to learn; however, we can learn good policies on the pupper in a day.

6. Discussion and Conclusion

In this work, we have created a new method for learning imitative policies from a single demonstration. The method uses a Siamese recurrent network to learn a distance function in both space and time. This distance function learns to imitate video data where the agent’s observed state can be noisy and partially observed. We use this model to provide rewards for training an RL policy. By using data from other motion styles and regularization terms, VIRL produces policies that demonstrate similar behaviour to the demonstration in complex 3D control tasks. We found that the recurrent distance learned by VIRL was particularly beneficial when imitating demonstrations with greater partial observability.

One might expect that the distance metric should be pretrained to quickly understand the difference between a good and bad demonstration. However, we have found that in this setting, learning too quickly can destabilize learning, as rewards can change, which can cause the agent to diverge off toward an unrecoverable policy space. In this setting, slower is better, as the distance metric may not yet be accurate. However, it may be locally or relatively reasonable, which is enough to learn an acceptable policy. As learning continues, these two optimizations can converge together.

When comparing our method to GAILfO, we have found that GAILfO has limited temporal consistency. GAILfO led to learning jerky and overactive policies. The use of a recurrent discriminator for GAILfO, similar to our use of sequence-based distance, may mitigate some of these issues and is left for future work. It is challenging to produce results better than the carefully manually crafted reward functions used by the RL simulation environments that include motion phase information in the observations (Peng et al., 2018a, 2017). However, we have shown that our method can compute distances in space and time and learns faster than current methods that can be used in this domain. A combination of beginning learning with our method and following with a manually crafted reward function could potentially lead to faster learning of high-quality policies if true state information is available. Still, as environments become increasingly more complex and real-world training becomes an efficient option, methods that can learn to imitate from only video enable access to a vast collection of motion information, extensive studies on multi-task learning, and give way to more natural methods to provide instructions to agents.

References

Pieter Abbeel and Andrew Y. Ng. Apprenticeship learning via inverse reinforcement learning. In *Proceedings of the Twenty-first International Conference on Machine Learning*,

- ICML '04, pages 1–, New York, NY, USA, 2004. ACM. ISBN 1-58113-838-5. doi: 10.1145/1015330.1015430. URL <http://doi.acm.org/10.1145/1015330.1015430>.
- Brenna D. Argall, Sonia Chernova, Manuela Veloso, and Brett Browning. A survey of robot learning from demonstration. *Robotics and Autonomous Systems*, 57(5):469 – 483, 2009. ISSN 0921-8890. doi: <https://doi.org/10.1016/j.robot.2008.10.024>. URL <http://www.sciencedirect.com/science/article/pii/S0921889008001772>.
- Sarah-Jayne Blakemore and Jean Decety. From the perception of action to the understanding of intention. *Nature reviews neuroscience*, 2(8):561–567, 2001.
- Daniel Brown, Wonjoon Goo, Prabhat Nagarajan, and Scott Niekum. Extrapolating beyond suboptimal demonstrations via inverse reinforcement learning from observations. In *International Conference on Machine Learning*, 2019.
- Daniel S Brown, Wonjoon Goo, and Scott Niekum. Better-than-demonstrator imitation learning via automatically-ranked demonstrations. In *Conference on Robot Learning*, pages 330–359, 2020.
- Yevgen Chebotar, Karol Hausman, Marvin Zhang, Gaurav Sukhatme, Stefan Schaal, and Sergey Levine. Combining model-based and model-free updates for trajectory-centric reinforcement learning. In *Proceedings of the 34th International Conference on Machine Learning-Volume 70*, pages 703–711, 2017.
- Sumit Chopra, Raia Hadsell, and Yann LeCun. Learning a similarity metric discriminatively, with application to face verification. In *Computer Vision and Pattern Recognition, 2005. CVPR 2005. IEEE Computer Society Conference on*, volume 1, pages 539–546. IEEE, 2005.
- D. Dwibedi, J. Tompson, C. Lynch, and P. Sermanet. Learning Actionable Representations from Visual Observations. *ArXiv e-prints*, August 2018.
- Ashley Edwards, Himanshu Sahni, Yannick Schroecker, and Charles Isbell. Imitating latent policies from observation. In *International Conference on Machine Learning*, pages 1755–1763, 2019.
- Chelsea Finn, Tianhe Yu, Justin Fu, Pieter Abbeel, and Sergey Levine. Generalizing skills with semi-supervised reinforcement learning. *CoRR*, abs/1612.00429, 2016. URL <http://arxiv.org/abs/1612.00429>.
- Chelsea Finn, Tianhe Yu, Tianhao Zhang, Pieter Abbeel, and Sergey Levine. One-shot visual imitation learning via meta-learning. *CoRR*, abs/1709.04905, 2017. URL <http://arxiv.org/abs/1709.04905>.
- Ian Goodfellow, Jean Pouget-Abadie, Mehdi Mirza, Bing Xu, David Warde-Farley, Sherjil Ozair, Aaron Courville, and Yoshua Bengio. Generative adversarial nets. In Z. Ghahramani, M. Welling, C. Cortes, N. D. Lawrence, and K. Q. Weinberger, editors, *Advances in Neural Information Processing Systems 27*, pages 2672–2680. Curran Associates, Inc., 2014. URL <http://papers.nips.cc/paper/5423-generative-adversarial-nets.pdf>.

- Raia Hadsell, Sumit Chopra, and Yann LeCun. Dimensionality reduction by learning an invariant mapping. In *2006 IEEE Computer Society Conference on Computer Vision and Pattern Recognition (CVPR'06)*, volume 2, pages 1735–1742. IEEE, 2006.
- K. He, X. Zhang, S. Ren, and J. Sun. Spatial pyramid pooling in deep convolutional networks for visual recognition. *IEEE Transactions on Pattern Analysis and Machine Intelligence*, 37(9):1904–1916, Sept 2015. ISSN 0162-8828. doi: 10.1109/TPAMI.2015.2389824.
- Jonathan Ho and Stefano Ermon. Generative adversarial imitation learning. In D. D. Lee, M. Sugiyama, U. V. Luxburg, I. Guyon, and R. Garnett, editors, *Advances in Neural Information Processing Systems 29*, pages 4565–4573. Curran Associates, Inc., 2016. URL <http://papers.nips.cc/paper/6391-generative-adversarial-imitation-learning.pdf>.
- Nathan Kau, Aaron Schultz, Tarun Punnoose, Laura Lee, and Zac Manchester. Woofers and puppers: Low-cost open-source quadrupeds for research and education. 2020.
- Diederik P Kingma and Max Welling. Auto-encoding variational bayes. *International Conference on Learning Representations (ICLR)*, 2014.
- Yunzhu Li, Jiaming Song, and Stefano Ermon. Infogail: Interpretable imitation learning from visual demonstrations. In I. Guyon, U. V. Luxburg, S. Bengio, H. Wallach, R. Fergus, S. Vishwanathan, and R. Garnett, editors, *Advances in Neural Information Processing Systems 30*, pages 3812–3822. Curran Associates, Inc., 2017. URL <http://papers.nips.cc/paper/6971-infogail-interpretable-imitation-learning-from-visual-demonstrations.pdf>.
- Yuxuan Liu, Abhishek Gupta, Pieter Abbeel, and Sergey Levine. Imitation from observation: Learning to imitate behaviors from raw video via context translation. *CoRR*, abs/1707.03374, 2017. URL <http://arxiv.org/abs/1707.03374>.
- Laurens van der Maaten and Geoffrey Hinton. Visualizing data using t-sne. *Journal of machine learning research*, 9(Nov):2579–2605, 2008.
- Josh Merel, Yuval Tassa, Dhruva TB, Sriram Srinivasan, Jay Lemmon, Ziyu Wang, Greg Wayne, and Nicolas Heess. Learning human behaviors from motion capture by adversarial imitation. *CoRR*, abs/1707.02201, 2017. URL <http://arxiv.org/abs/1707.02201>.
- Ashvin Nair, Vitchyr Pong, Murtaza Dalal, Shikhar Bahl, Steven Lin, and Sergey Levine. Visual reinforcement learning with imagined goals. *CoRR*, abs/1807.04742, 2018. URL <http://arxiv.org/abs/1807.04742>.
- Andrew Y Ng, Stuart J Russell, et al. Algorithms for inverse reinforcement learning. In *Icml*, volume 1, page 2, 2000.
- Deepak Pathak, Parsa Mahmoudieh, Guanghao Luo, Pulkit Agrawal, Dian Chen, Yide Shentu, Evan Shelhamer, Jitendra Malik, Alexei A. Efros, and Trevor Darrell. Zero-shot visual imitation. *CoRR*, abs/1804.08606, 2018. URL <http://arxiv.org/abs/1804.08606>.

- Xue Bin Peng and Michiel van de Panne. Learning locomotion skills using deeprl: Does the choice of action space matter? In *Proceedings of the ACM SIGGRAPH / Eurographics Symposium on Computer Animation*, SCA '17, pages 12:1–12:13, New York, NY, USA, 2017. ACM. ISBN 978-1-4503-5091-4. doi: 10.1145/3099564.3099567. URL <http://doi.acm.org/10.1145/3099564.3099567>.
- Xue Bin Peng, Glen Berseth, Kangkang Yin, and Michiel Van De Panne. Deeploco: Dynamic locomotion skills using hierarchical deep reinforcement learning. *ACM Trans. Graph.*, 36(4):41:1–41:13, July 2017. ISSN 0730-0301. doi: 10.1145/3072959.3073602. URL <http://doi.acm.org/10.1145/3072959.3073602>.
- Xue Bin Peng, Pieter Abbeel, Sergey Levine, and Michiel van de Panne. Deepmimic: Example-guided deep reinforcement learning of physics-based character skills. *ACM Trans. Graph.*, 37(4):143:1–143:14, July 2018a. ISSN 0730-0301. doi: 10.1145/3197517.3201311. URL <http://doi.acm.org/10.1145/3197517.3201311>.
- Xue Bin Peng, Angjoo Kanazawa, Sam Toyer, Pieter Abbeel, and Sergey Levine. Variational discriminator bottleneck: Improving imitation learning, inverse rl, and gans by constraining information flow. *arXiv preprint arXiv:1810.00821*, 2018b.
- Xue Bin Peng, Erwin Coumans, Tingnan Zhang, Tsang-Wei Edward Lee, Jie Tan, and Sergey Levine. Learning agile robotic locomotion skills by imitating animals. In *Robotics: Science and Systems*, 07 2020. doi: 10.15607/RSS.2020.XVI.064.
- Xue Bin Peng, Ze Ma, Pieter Abbeel, Sergey Levine, and Angjoo Kanazawa. Amp: Adversarial motion priors for stylized physics-based character control. *ACM Trans. Graph.*, 40(4), July 2021. doi: 10.1145/3450626.3459670. URL <http://doi.acm.org/10.1145/3450626.3459670>.
- Stephane Ross, Geoffrey Gordon, and Drew Bagnell. A reduction of imitation learning and structured prediction to no-regret online learning. In Geoffrey Gordon, David Dunson, and Miroslav Dudík, editors, *Proceedings of the Fourteenth International Conference on Artificial Intelligence and Statistics*, volume 15 of *Proceedings of Machine Learning Research*, pages 627–635, Fort Lauderdale, FL, USA, 11–13 Apr 2011a. PMLR. URL <http://proceedings.mlr.press/v15/ross11a.html>.
- Stéphane Ross, Geoffrey Gordon, and Drew Bagnell. A reduction of imitation learning and structured prediction to no-regret online learning. In *Proceedings of the fourteenth international conference on artificial intelligence and statistics*, pages 627–635, 2011b.
- John Schulman, Sergey Levine, Pieter Abbeel, Michael Jordan, and Philipp Moritz. Trust region policy optimization. In *International conference on machine learning*, pages 1889–1897, 2015.
- Pierre Sermanet, Corey Lynch, Jasmine Hsu, and Sergey Levine. Time-contrastive networks: Self-supervised learning from multi-view observation. *CoRR*, abs/1704.06888, 2017. URL <http://arxiv.org/abs/1704.06888>.

- Pierre Sermanet, Corey Lynch, Yevgen Chebotar, Jasmine Hsu, Eric Jang, Stefan Schaal, Sergey Levine, and Google Brain. Time-contrastive networks: Self-supervised learning from video. In *2018 IEEE International Conference on Robotics and Automation (ICRA)*, pages 1134–1141. IEEE, 2018.
- Pratyusha Sharma, Deepak Pathak, and Abhinav Gupta. Third-person visual imitation learning via decoupled hierarchical controller. In H. Wallach, H. Larochelle, A. Beygelzimer, F. d’Alché-Buc, E. Fox, and R. Garnett, editors, *Advances in Neural Information Processing Systems 32*, pages 2597–2607. Curran Associates, Inc., 2019. URL <http://papers.nips.cc/paper/8528-third-person-visual-imitation-learning-via-decoupled-hierarchical-controller.pdf>.
- Wen Sun, Anirudh Vemula, Byron Boots, and Drew Bagnell. Provably efficient imitation learning from observation alone. In *ICML*, pages 6036–6045, 2019. URL <http://proceedings.mlr.press/v97/sun19b.html>.
- Faraz Torabi, Garrett Warnell, and Peter Stone. Behavioral Cloning from Observation. (July), 2018a. URL <http://arxiv.org/abs/1805.01954>.
- Faraz Torabi, Garrett Warnell, and Peter Stone. Generative adversarial imitation from observation. *arXiv preprint arXiv:1807.06158*, 2018b.
- Ziyu Wang, Josh S Merel, Scott E Reed, Nando de Freitas, Gregory Wayne, and Nicolas Heess. Robust imitation of diverse behaviors. In I. Guyon, U. V. Luxburg, S. Bengio, H. Wallach, R. Fergus, S. Vishwanathan, and R. Garnett, editors, *Advances in Neural Information Processing Systems 30*, pages 5320–5329. Curran Associates, Inc., 2017. URL <http://papers.nips.cc/paper/7116-robust-imitation-of-diverse-behaviors.pdf>.
- Chao Yang, Xiaojian Ma, Wenbing Huang, Fuchun Sun, Huaping Liu, Junzhou Huang, and Chuang Gan. Imitation learning from observations by minimizing inverse dynamics disagreement. In H. Wallach, H. Larochelle, A. Beygelzimer, F. d’Alché-Buc, E. Fox, and R. Garnett, editors, *Advances in Neural Information Processing Systems 32*, pages 239–249. Curran Associates, Inc., 2019. URL <http://papers.nips.cc/paper/8317-imitation-learning-from-observations-by-minimizing-inverse-dynamics-disagreement.pdf>.
- Tianhe Yu, Chelsea Finn, Annie Xie, Sudeep Dasari, Tianhao Zhang, Pieter Abbeel, and Sergey Levine. One-shot imitation from observing humans via domain-adaptive meta-learning. *CoRR*, abs/1802.01557, 2018. URL <http://arxiv.org/abs/1802.01557>.
- Zhuotun Zhu, Xinggang Wang, Song Bai, Cong Yao, and Xiang Bai. Deep learning representation using autoencoder for 3d shape retrieval. *Neurocomputing*, 204:41–50, 2016.
- Fuzhen Zhuang, Xiaohu Cheng, Ping Luo, Sinno Jialin Pan, and Qing He. Supervised representation learning: Transfer learning with deep autoencoders. In *Twenty-Fourth International Joint Conference on Artificial Intelligence*, 2015.

Brian D. Ziebart, Andrew Maas, J. Andrew Bagnell, and Anind K. Dey. Maximum entropy inverse reinforcement learning. In *Proceedings of the 23rd National Conference on Artificial Intelligence - Volume 3*, AAAI'08, pages 1433–1438. AAAI Press, 2008. ISBN 978-1-57735-368-3. URL <http://dl.acm.org/citation.cfm?id=1620270.1620297>.

7. Appendix

This section includes additional details related to VIRL.

7.1 Imitation Learning

Imitation learning is the process of training a new policy to reproduce the behaviour of some expert policy. BC is a fundamental method for imitation learning. Given an expert policy π_E possibly represented as a collection of trajectories $\tau < (s_0, a_0), \dots, (s_T, a_T) >$ a new policy π can be learned to match these trajectory using supervised learning.

$$\max_{\theta} \mathbb{E}_{\pi_E} \left[\sum_{t=0}^T \log \pi(a_t | s_t, \theta_{\pi}) \right] \quad (5)$$

While this simple method can work well, it often suffers from distribution mismatch issues leading to compounding errors as the learned policy deviates from the expert’s behaviour during test time.

7.2 Inverse Reinforcement Learning

Similar to BC, Inverse Reinforcement Learning (inverse reinforcement learning (IRL)) also learns to replicate some desired, potentially expert, behaviour. However, IRL uses the RL environment to learn a reward function that learns to tell the difference between the agent’s behaviour and the example data. Here we describe maximal entropy IRL (Ziebart et al., 2008). Given an expert trajectory $\tau < (s_0, a_0), \dots, (s_T, a_T) >$ a policy π can be trained to produce similar trajectories by discovering a distance metric between the expert trajectory and trajectories produced by the policy π .

$$\max_{c \in C} \min_{\pi} (\mathbb{E}_{\pi} [c(s, a)] - H(\pi)) - \mathbb{E}_{\pi_E} [c(s, a)] \quad (6)$$

where c is some learned cost function and $H(\pi)$ is a causal entropy term. π_E is the expert policy that is represented by a collection of trajectories. IRL is searching for a cost function c that is low for the expert π_E and high for other policies. Then, a policy can be optimized by maximizing the reward function $r_t = -c(s_t, a_t)$.

7.3 Data

We are using the mocap data from the “CMU Graphics Lab Motion Capture Database” from 2002 (<http://mocap.cs.cmu.edu/>). To be thorough, we provide the process at length. This data has been preprocessed to map the mocap markers to a human skeleton. Each recording contains the positions and orientations of the different joints of a human skeleton and can therefore directly be used to animate a humanoid mesh. This is a standard approach that has been widely used in prior literature [Gleicher 1998, Rosales 2000, Lee 2002]. To be precise: at each mocap frame, the joints of a humanoid mesh model are set to the positions and orientations of their respective values in the recording. If a full humanoid mesh is not available, it is possible to add capsule mesh primitives between each recorded joint. This 3D mesh model is then rendered to an image through a 3rd person camera that follows the center of mass of the mesh at a fixed distance.



Figure 11: Rasterized frames of the imitation motions on humanoid3d walking (row 1), running (row 2), zombie (row 3) and jumping (row 4). <https://sites.google.com/view/virl1>

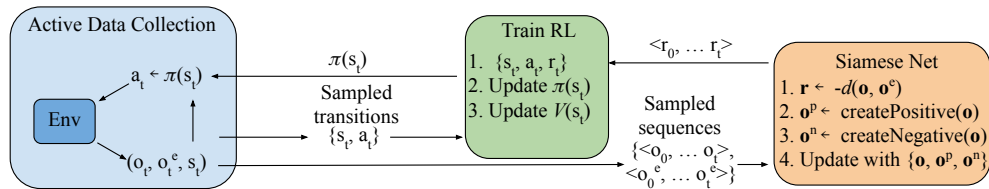


Figure 12: The flow of control for the learning system.

For the humanoid experiments, imitation data for 24 other tasks was used to help condition the distance metric learning process. These include motion clips for running, backflips, frontflips, dancing, punching, kicking and jumping along with the desired motion. The improvement due to these additional unsupervised training data generation mechanisms are shown in Fig. 8a.

7.4 Training Details

The learning simulations are trained using graphics processing unit (GPU)s. The simulation is not only simulating the interaction physics of the world but also rendering the simulation scene to capture video observations. On average, it takes 3 days to execute a single training simulation. The rendering process and copying the images from the GPU is one of the most expensive operations with VIRL. We collect 2048 samples between training rounds. The batch size for TRPO is 2048. The kl term is 0.5.

The simulation environment includes several different tasks represented by a collection of motion capture clips to imitate. These tasks come from the tasks created in DeepMimic (Peng et al., 2018a). We include all humanoid tasks in this dataset.

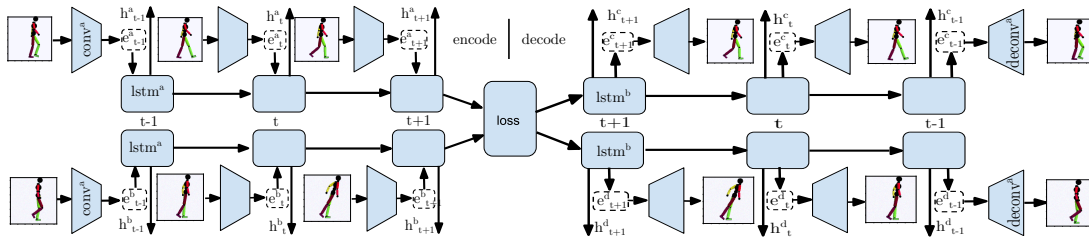


Figure 13: We use a Siamese autoencoding network structure that can provide a reward signal at every step to a reinforcement learning algorithm. For the Humanoid experiments here, the convolutional portion of our network includes 2 convolution layers of 8 filters with size 6×6 and stride 2×2 , 16 filters of size 4×4 and stride 2×2 . The features are then flattened and followed by two dense layers of 256 and 64 units. The majority of the network uses Rectified Linear Unit (ReLU) activations except for the last layer that uses a sigmoid activation. Dropout is used between convolutional layers. The RNN-based model uses a LSTM layer with 128 hidden units, followed by a dense layer of 64 units. The decoder model has the same structure in reverse, with deconvolution in place of convolutional layers.

In Alg. 1 we include an outline of the algorithm used for the method and a diagram in Fig. 12. The simulation environment produces three types of observations, s_{t+1} the agent’s proprioceptive pose, s_{t+1}^v the image observation of the agent and m_{t+1} the image-based observation of the expert demonstration. The images are grayscale 64×64 .

7.5 Distance Function Training

In Fig. 14a, the learning curve for the Siamese RNN is shown during a pretraining phase. We can see the overfitting portion that occurs during RL training. This overfitting can lead to poor reward prediction during the early phase of training. In Fig. 14b, we show the training curve for the recurrent Siamese network after starting training during RL. After an initial distribution adaptation, the model learns smoothly, considering that the training data used is continually changing as the RL agent explores.

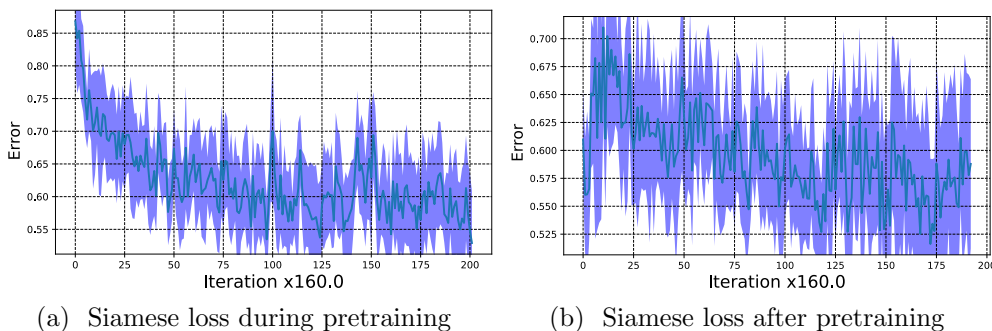


Figure 14: Training losses for the Siamese distance metric.

It can be challenging to train a sequenced-based distance function. One particular challenge is training the distance function to be accurate across the space of possible states. We found that a good strategy was to focus on the earlier parts of the episode. When the model is not accurate on states earlier in the episode, it may never learn how to get into

good states later, even if the distance function understands those better. Therefore, when constructing batches to train the RNN on, we give a higher probability of starting earlier in episodes. We also give a higher probability of shorter sequences as a function of the average episode length. As the agent gets better average episode length increases, so to will the randomly selected sequence windows.

7.6 Distance Function Use

We find it helpful to *normalize* the distance metric outputs using $r = \exp(r^2 * w_d)$ where $w_d = -5.0$ scales the filtering width. This normalization is a standard method to convert distance-based rewards to be positive, which makes it easier to handle episodes that terminate early (Peng et al., 2018a,b; Peng and van de Panne, 2017). Early in training, the distance metric often produces large, noisy values. The RL method regularly tracks reward scaling statistics; the initial high variance data reduces the significance of better distance metric values produced later on by scaling them to small numbers. The improvement of using this normalized reward is shown in Fig. 15a. In Fig. 15b we compare to a few baseline methods. The *manual* version uses a carefully engineered reward function from (Peng et al., 2017).

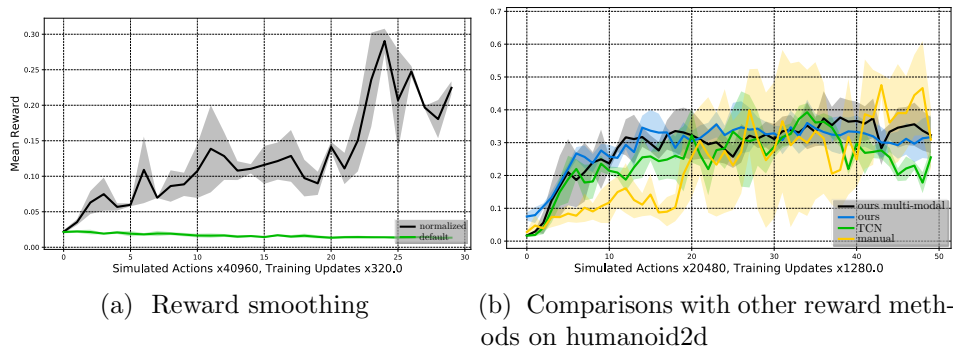


Figure 15: Ablation analysis of VIRL. We find that training RL policies is sensitive to the size and distribution of rewards. We compare VIRL to several baselines.

7.7 Positive and Negative Examples

We use two methods to generate positive and negative examples. The first method is similar to TCN, where we can assume that sequences that overlap more in time are more similar. We generate two sequences for each episode, one for the agent and one for the imitation motion. Here we list the methods used to alter sequences for positive pairs.

1. Adding Gaussian noise to each state in the sequence (mean = 0 and variance = 0.02)
2. Out of sync versions where the first state from the first and the last ones from the second sequence are removed.
3. Duplicating the first state in either sequence
4. Duplicating the last state in either sequence

We alter sequences for negative pairs by

1. Reversing the ordering of the second sequence in the pair.
2. Randomly picking a state out of the second sequence and replicating it to be as long as the first sequence.
3. Randomly shuffling one sequence.
4. Randomly shuffling both sequences.

The second method we use to create positive and negative examples is by including data for additional classes of motion. These classes denote different task types. For the humanoid3d environment, we generate data for walking-dynamic-speed, running, backflipping and front-flipping. Pairs from the same tasks are labelled as positive, and pairs from different classes are negative.